

Entropy stable modal discontinuous Galerkin schemes and wall boundary conditions for the compressible Navier-Stokes equations

Jesse Chan^a, Yimin Lin^a, Tim Warburton^b

^a*Department of Computational and Applied Mathematics, Rice University, 6100 Main St, Houston, TX, 77005*

^b*Department of Mathematics, Virginia Tech, 225 Stanger Street, Blacksburg, VA 24061-1026*

Abstract

Entropy stable schemes ensure that physically meaningful numerical solutions also satisfy a semi-discrete entropy inequality under appropriate boundary conditions. In this work, we describe a discretization of viscous terms in the compressible Navier-Stokes equations which enables a simple and explicit imposition of entropy stable no-slip (adiabatic and isothermal) and reflective (symmetry) wall boundary conditions for discontinuous Galerkin (DG) discretizations. Numerical results confirm the robustness and accuracy of the proposed approaches.

1. Introduction

Computational fluid dynamics (CFD) has relied mainly on first and second order numerical methods, which are robust and reliable. However, because higher order schemes offer improved accuracy at similar computational costs, they have received significant interest as demand for greater resolution in engineering simulations increases [1]. Discontinuous Galerkin (DG) schemes are among the most popular high order schemes for CFD, especially for transient vortical flows [2, 3]. However, high order methods typically suffer from issues of robustness, especially in the presence of shocks and under-resolved solution features. Entropy stable high order DG schemes [4, 5, 6, 7, 8] provide one way to improve robustness without sacrificing high order accuracy. This improved robustness can be attributed to the fact that entropy stable schemes are stable in the sense that they satisfy a semi-discrete entropy inequality, even in the presence of aliasing errors resulting from under-integration, nonlinear fluxes, and curved geometries [9].

Entropy stable DG schemes for the compressible Euler and Navier-Stokes equations were introduced for tensor product (quadrilateral and hexahedral) meshes by Carpenter et al. in [4] and Gassner, Winters, and Kopriva in [5]. The construction of such schemes utilized connections between nodal DG spectral element methods (DG-SEM) and summation by parts (SBP) finite difference operators. These schemes were later extended to simplicial meshes in [6, 7] based on a generalization of SBP operators to the multi-dimensional case [10]. Entropy stable schemes were then extended to more general “modal” DG formulations in [8, 11, 12]. Other recent entropy stable numerical schemes include staggered grid schemes [13, 14], collocation schemes based on Gauss points [15, 16], and entropy stable reduced order models [17]. Entropy stable schemes have also

Email addresses: jesse.chan@rice.edu (Jesse Chan), yiminlin@rice.edu (Yimin Lin), tcew@vt.edu (Tim Warburton)

been extended to the fully discrete case using entropy conservative and entropy stable relaxation Runge-Kutta time-stepping methods [18, 19].

For periodic domains, entropy stable schemes automatically guarantee the satisfaction of a semi-discrete entropy inequality. However, for non-periodic domains, entropy stable schemes must also be paired with appropriate entropy stable boundary conditions. Boundary conditions for DG schemes are typically imposed through the solution of appropriate Riemann problems [20], though not all such boundary conditions are entropy stable. The stability of boundary conditions for the compressible Navier-Stokes equations has typically been analyzed based on a linearized stability analysis [21]; however, linearly stable boundary conditions do not necessarily imply entropy stability either. Instead, more recent work has focused on the construction of nonlinearly stable boundary conditions for the compressible Euler and Navier-Stokes equations. Inviscid entropy stable wall and far-field boundary conditions for the compressible Euler equations were investigated in [22, 6], and viscous entropy stable adiabatic wall boundary conditions were analyzed in [23, 24, 25].

In this work, we focus on the construction of viscous wall boundary conditions for the compressible Navier-Stokes equations which mimic the continuous entropy balance. The key novelty of this work is a modified DG discretization of the viscous terms which simplifies methods for imposing viscous wall boundary conditions. In [23, 24, 25], viscous wall boundary conditions are imposed by transforming between conservative and primitive variables. In this work, we introduce a modified viscous discretization which is more amenable to modal DG discretizations. We also show this formulation enables the imposition of no-slip wall boundary conditions in a simple and explicit fashion while also providing simpler proofs of entropy conservation. Finally, we derive an entropy stable imposition of reflective symmetry boundary conditions on the viscous stresses, which have not yet been treated in the literature on entropy stable schemes.

The outline of the paper is as follows: Section 2 reviews entropy stability theory for the compressible Navier-Stokes equations, and Section 3 reviews the construction of entropy stable high order “modal” DG methods. Section 4 describes the the imposition of adiabatic, isothermal, no-slip, and symmetry wall boundary conditions which mimic the continuous entropy balance, and discusses the construction of boundary penalization terms. Section 5 provides numerical experiments which verify our theoretical results, and we provide conclusions and outlook in Section 6.

2. Entropy stability for the compressible Navier-Stokes equations

Let \mathbf{u} denote the vector of conservative variables. In two dimensions, these are

$$\mathbf{u} = \{\rho, \rho u_1, \dots, \rho u_d, E\} \in \mathbb{R}^{d+2}.$$

Here, ρ is density, u_i denotes the velocity in the i th coordinate direction, and E denotes the specific total energy. We also introduce the pressure p and temperature T , which are related to the conservative variables through the constitutive relations

$$p = (\gamma - 1)\rho e, \quad E = e + \frac{1}{2} \sum_{i=1}^d u_i^2, \quad e = c_v T,$$

where $\gamma = 1.4$, e is the internal energy density, and c_v is the specific heat at constant volume. Pr denotes the Prandtl number, and μ, λ are the dynamic and bulk viscosity coefficients, respectively.

The compressible Navier-Stokes equations in d dimensions are given by

$$\frac{\partial \mathbf{u}}{\partial t} + \sum_{i=1}^d \frac{\partial \mathbf{f}_i}{\partial x_i} = \sum_{i=1}^d \frac{\partial \mathbf{g}_i}{\partial x_i}, \quad (1)$$

where \mathbf{f}_i denote the inviscid fluxes in the i th coordinate direction.

In this work, we focus on the two-dimensional compressible Navier-Stokes equations. However, the main contributions of this paper are straightforward to extend to three dimensions, and we present results in a dimension-independent manner when possible. For $d = 2$, the inviscid fluxes \mathbf{f}_i are given by

$$\mathbf{f}_1 = \begin{bmatrix} \rho u_1 \\ \rho u_1^2 + p \\ \rho u_1 u_2 \\ u_1(E + p) \end{bmatrix}, \quad \mathbf{f}_2 = \begin{bmatrix} \rho u_2 \\ \rho u_1 u_2 \\ \rho u_2^2 + p \\ u_2(E + p) \end{bmatrix}$$

The viscous fluxes $\mathbf{g}_1, \mathbf{g}_2$ for $d = 2$ are given by

$$\mathbf{g}_1 = \begin{bmatrix} 0 \\ \tau_{1,1} \\ \tau_{2,1} \\ \sum_{i=1}^d \tau_{i,1} u_i - \kappa \frac{\partial T}{\partial x_1} \end{bmatrix}, \quad \mathbf{g}_2 = \begin{bmatrix} 0 \\ \tau_{1,2} \\ \tau_{2,2} \\ \sum_{i=1}^d \tau_{i,2} u_i - \kappa \frac{\partial T}{\partial x_2} \end{bmatrix}. \quad (2)$$

Here, $\kappa = \kappa(T)$ denotes the thermal conductivity, and $\tau_{i,j}$ denote the components of the viscous stress tensor

$$\tau_{i,j} = \mu \left(\frac{\partial u_i}{\partial x_j} + \frac{\partial u_j}{\partial x_i} \right) - \delta_{ij} \lambda \left(\sum_{i=1}^d \frac{\partial u_i}{\partial x_i} \right), \quad 1 \leq i, j \leq d. \quad (3)$$

We assume Stokes hypothesis in this work, or that $\lambda = \frac{2}{3}\mu$.

2.1. Nondimensionalization

We follow [26] and introduce nondimensional quantities for length, density, velocity, temperature, and viscosity

$$\mathbf{x}^* = \frac{\mathbf{x}}{L}, \quad \rho^* = \frac{\rho}{\rho_\infty}, \quad T^* = \frac{T}{T_\infty}, \quad \mu^* = \frac{\mu}{\mu_\infty} \quad (4)$$

$$u_i = \frac{u_i}{U_\infty}, \quad i = 1, \dots, d. \quad (5)$$

We can then non-dimensionalize pressure, internal energy, and bulk viscosity with respect to combinations of reference quantities

$$p^* = \frac{p}{\rho_\infty U_\infty^2}, \quad e = \frac{e}{U_\infty^2}, \quad \lambda^* = \frac{\lambda}{\mu_\infty}.$$

We introduce the Reynolds and free-stream Mach numbers

$$\text{Re} = \frac{\rho_\infty U_\infty L}{\mu_\infty}, \quad \text{Ma} = \frac{U_\infty}{\sqrt{\gamma(\gamma-1)c_v T_\infty}}. \quad (6)$$

Note that the reference Mach number is the ratio of the free-stream velocity to the free-stream speed of sound a_∞

$$a_\infty = \sqrt{\frac{\gamma p_\infty}{\rho_\infty}} = \sqrt{\gamma(\gamma-1)c_v T_\infty},$$

since $p = (\gamma-1)\rho e$ and $e = c_v T$.

The non-dimensionalized equations take the same form as the original equations if we define new physical parameters

$$\tilde{\mu} = \frac{\mu^*}{\text{Re}}, \quad \tilde{\lambda} = \frac{\lambda^*}{\text{Re}}, \quad \tilde{c}_v = \frac{1}{\gamma(\gamma-1)\text{Ma}^2}, \quad \tilde{\kappa} = \frac{\gamma \tilde{c}_v \tilde{\mu}}{\text{Pr}}.$$

From this point on, we drop both the tilde and the * superscript and assume all variables to refer to their nondimensionalized quantities.

2.2. Entropy variables and symmetrization

The compressible Navier-Stokes equations admit a mathematical entropy inequality with respect to the convex scalar entropy function $S(\mathbf{u})$

$$S(\mathbf{u}) = -\rho s,$$

where $s = \log\left(\frac{p}{\rho^\gamma}\right)$ denotes the physical entropy [27]. The derivative of the entropy with respect to the conservative variables yield the entropy variables $\mathbf{v}(\mathbf{u}) = \frac{\partial S}{\partial \mathbf{u}} = \{v_1, v_2, v_3, v_4\}$, where

$$v_1 = \frac{\rho e(\gamma+1-s) - E}{\rho e}, \quad v_{1+i} = \frac{\rho u_i}{\rho e}, \quad v_{d+2} = -\frac{\rho}{\rho e} \quad (7)$$

for $i = 1, \dots, d$. The inverse mapping is given by

$$\rho = -(\rho e)v_{d+2}, \quad \rho u_i = (\rho e)v_{1+i}, \quad E = (\rho e) \left(1 - \frac{\sum_{j=1}^d v_{1+j}^2}{2v_{d+2}} \right),$$

where $i = 1, \dots, d$, and ρe and s in terms of the entropy variables are

$$\rho e = \left(\frac{(\gamma-1)}{(-v_{d+2})^\gamma} \right)^{1/(\gamma-1)} e^{\frac{-s}{\gamma-1}}, \quad s = \gamma - v_1 + \frac{\sum_{j=1}^d v_{1+j}^2}{2v_{d+2}}.$$

It was shown in [27] that the entropy variables *symmetrizes* the viscous fluxes in the sense that

$$\sum_{i=1}^d \frac{\partial \mathbf{g}_i}{\partial x_i} = \sum_{i,j=1}^d \frac{\partial}{\partial x_i} \left(\mathbf{K}_{ij} \frac{\partial \mathbf{v}}{\partial x_j} \right). \quad (8)$$

where \mathbf{K}_{ij} denote blocks of a symmetric and positive semi-definite matrix \mathbf{K}

$$\mathbf{K} = \begin{bmatrix} \mathbf{K}_{11} & \dots & \mathbf{K}_{1d} \\ \vdots & \ddots & \vdots \\ \mathbf{K}_{d1} & \dots & \mathbf{K}_{dd} \end{bmatrix} = \mathbf{K}^T, \quad \mathbf{K} \succeq 0.$$

Formulas for these matrices for $d = 2$ are given in terms of the entropy variables and physical parameters

$$\begin{aligned}
K_{11} &= \frac{1}{v_4^3} \begin{pmatrix} 0 & 0 & 0 & 0 \\ 0 & -(\lambda + 2\mu)v_4^2 & 0 & (\lambda + 2\mu)v_2v_4 \\ 0 & 0 & -\mu v_4^2 & \mu v_3v_4 \\ 0 & (\lambda + 2\mu)v_2v_4 & \mu v_3v_4 & -[(\lambda + 2\mu)v_2^2 + \mu(v_3^2) - \gamma\mu v_4/Pr] \end{pmatrix} \\
K_{12} &= \frac{1}{v_4^3} \begin{pmatrix} 0 & 0 & 0 & 0 \\ 0 & 0 & -\lambda v_4^2 & \lambda v_3v_4 \\ 0 & -\mu v_4^2 & 0 & \mu v_2v_4 \\ 0 & \mu v_3v_4 & \lambda v_2v_4 & (\lambda + \mu)(-v_2v_3) \end{pmatrix} \\
K_{21} &= \frac{1}{v_4^3} \begin{pmatrix} 0 & 0 & 0 & 0 \\ 0 & 0 & -\mu v_4^2 & \mu v_3v_4 \\ 0 & -\lambda v_4^2 & 0 & \lambda v_2v_4 \\ 0 & \lambda v_3v_4 & \mu v_2v_4 & (\lambda + \mu)(-v_2v_3) \end{pmatrix} \\
K_{22} &= \frac{1}{v_4^3} \begin{pmatrix} 0 & 0 & 0 & 0 \\ 0 & -\mu v_4^2 & 0 & \mu v_2v_4 \\ 0 & 0 & -(\lambda + 2\mu)v_4^2 & (\lambda + 2\mu)v_3v_4 \\ 0 & \mu v_2v_4 & (\lambda + 2\mu)v_3v_4 & -[(\lambda + 2\mu)v_3^2 + \mu(v_2^2) - \gamma\mu v_4/Pr] \end{pmatrix}
\end{aligned}$$

Similar formulas for the symmetrized matrices \mathbf{K}_{ij} in three-dimensions are derived in [27].

2.3. Continuous entropy balance

An entropy balance equation can be derived by multiplying the compressible Navier-Stokes equations by the entropy variables and integrating over the domain. We begin by introducing a few related identities. It can be shown that the following identity is satisfied

$$\begin{aligned}
\mathbf{v}^T \frac{\partial \mathbf{f}_i(\mathbf{u})}{\partial x_i} &= \frac{\partial F_i(\mathbf{u})}{\partial x_i} \\
F_i(\mathbf{u}) &= \mathbf{v}(\mathbf{u})^T \mathbf{f}_i(\mathbf{u}) - \psi_i(\mathbf{u}),
\end{aligned} \tag{9}$$

where $F_i(\mathbf{u})$ and $\psi_i(\mathbf{u})$ denote scalar entropy fluxes and potentials, respectively. For the compressible Navier-Stokes equations, $F_i(\mathbf{u})$ and $\psi_i(\mathbf{u})$ are given by [27, 6]

$$F_i(\mathbf{u}) = -\frac{s\rho u_i}{\gamma - 1}, \quad \psi_i(\mathbf{u}) = \rho u_i.$$

Multiplying (1) by \mathbf{v}^T , integrating over Ω , and using the chain rule and aforementioned identities then yields

$$\int_{\Omega} \frac{\partial S(\mathbf{u})}{\partial t} + \int_{\partial\Omega} \sum_{i=1}^d (F_i(\mathbf{u}) - \mathbf{v}^T \mathbf{g}_i) n_i + \int_{\Omega} \sum_{i,j=1}^d \left(\frac{\partial \mathbf{v}}{\partial x_i} \right)^T \left(\mathbf{K}_{i,j} \frac{\partial \mathbf{v}}{\partial x_j} \right) = 0. \tag{10}$$

Using that $e = c_v T$, along with definitions of the entropy variables and viscous fluxes \mathbf{g}_i , we can show that the boundary contributions $\mathbf{v}^T \mathbf{g}_i$ reduce to a scaling by c_v of the quantity known as “heat entropy flow” [25]

$$\mathbf{v}^T \mathbf{g}_i = \frac{1}{c_v T} \kappa \frac{\partial T}{\partial x_i}. \tag{11}$$

Thus, the entropy balance for the compressible Navier-Stokes equations is

$$\int_{\Omega} \frac{\partial S(\mathbf{u})}{\partial t} = \int_{\partial\Omega} \sum_{i=1}^d \left(\frac{1}{c_v T} \kappa \frac{\partial T}{\partial x_i} - F_i(\mathbf{u}) \right) n_i - \int_{\Omega} \sum_{i,j=1}^d \left(\frac{\partial \mathbf{v}}{\partial x_i} \right)^T \left(\mathbf{K}_{i,j} \frac{\partial \mathbf{v}}{\partial x_j} \right). \quad (12)$$

Since the latter term involving $\mathbf{K}_{i,j}$ is non-positive, we can bound the rate of change of the integrated entropy by

$$\int_{\Omega} \frac{\partial S(\mathbf{u})}{\partial t} \leq \int_{\partial\Omega} \sum_{i=1}^d \left(\frac{1}{c_v T} \kappa \frac{\partial T}{\partial x_i} - F_i(\mathbf{u}) \right) n_i. \quad (13)$$

For certain boundary conditions, both the inviscid and viscous boundary terms in (13) vanish [22, 23, 6, 24, 25], implying that the solution is entropy stable. More generally, the goal of this work will be to impose boundary conditions such that the semi-discrete entropy inequality mimics the continuous entropy balance (12).

3. Entropy stable modal DG discretizations

3.1. On notation

The notation in this paper is motivated by notation in [7, 28]. Unless otherwise specified, vector and matrix quantities are denoted using lower and upper case bold font, respectively. Spatially discrete quantities are denoted using a bold sans serif font. Finally, the output of continuous functions evaluated over discrete vectors is interpreted as a discrete vector.

For example, if \mathbf{x} denotes a vector of point locations, i.e., $(\mathbf{x})_i = \mathbf{x}_i$, then $u(\mathbf{x})$ is interpreted as the vector

$$(u(\mathbf{x}))_i = u(\mathbf{x}_i).$$

Similarly, if $\mathbf{u} = u(\mathbf{x})$, then $f(\mathbf{u})$ corresponds to the vector

$$(f(\mathbf{u}))_i = f(u(\mathbf{x}_i)).$$

Vector-valued functions are treated similarly. For example, given a vector-valued function $\mathbf{f} : \mathbb{R}^n \rightarrow \mathbb{R}^n$ and a vector of coordinates \mathbf{x} , we adopt the convention that $(\mathbf{f}(\mathbf{x}))_i = \mathbf{f}(\mathbf{x}_i)$.

3.2. Modal DG discretizations

We now discuss the construction of an entropy stable DG discretization for the compressible Navier-Stokes equations. For generality, we assume a “modal” framework which is applicable to a broad range of approximation spaces and quadrature rules. We assume the domain Ω can be decomposed into non-overlapping elements D^k , each of which is the image of a reference element \widehat{D} under an invertible mapping Φ^k . Let \widehat{n}_i denote the i th component of the outward normal vector on the boundary of the reference element $\partial\widehat{D}$, and let \widehat{J}_f denote the determinant of the Jacobian of the transformation between a face of \widehat{D} and some reference face. Let $\widehat{\mathbf{x}}, \mathbf{x}$ denote coordinates on the reference element \widehat{D} and physical element D^k , respectively, such that

$$\widehat{\mathbf{x}} = \{\widehat{x}_1, \dots, \widehat{x}_d\}, \quad \mathbf{x} = \{x_1, \dots, x_d\}. \quad (14)$$

We also assume that the boundary of each element D^k is denoted by ∂D^k , and that the outward unit normal on each face in ∂D^k is denoted by $\mathbf{n} = \{n_1, \dots, n_d\}$. Finally, let J^k denote the determinant of the Jacobian of the mapping Φ^k , and let J_f^k denote the determinant of the Jacobian of the mapping from a face of ∂D^k to a reference face.

Local approximation spaces on each physical element D^k are defined as mappings of a reference approximation space. For this work, we assume \widehat{D} is the bi-unit right triangle and that the reference approximation space is the space of total degree N polynomials

$$P^N = \left\{ \widehat{x}_1^i \widehat{x}_2^j, \quad i, j \geq 0, \quad i + j \leq N \right\}$$

where \widehat{x}_i denotes the i th coordinate on the reference element.

Next, we introduce notation for jumps and averages of functions across element interfaces. Let $u(\mathbf{x})$ be a scalar function on D^k , and let u, u^+ denote its ‘‘interior’’ and ‘‘exterior’’ values across the face shared by neighbor $D^{k,+}$

$$\{\{u\}\} = \frac{u^+ + u}{2}, \quad \llbracket u \rrbracket = u^+ - u.$$

The jump and average of vector-valued functions are defined component-wise. Boundary conditions are also imposed by specifying appropriate exterior values.

We also assume volume and surface quadrature rules which are exact for degree $2N$ polynomials. Let $\{\mathbf{x}_i, w_i\}_{i=1}^{N_q}$ denote the points and weights of the volume quadrature rule, and let $\{\mathbf{x}_i^f, w_i^f\}_{i=1}^{N_q^f}$ denote the points and weights of the surface quadrature rule. Now, let $\{\phi_i(\mathbf{x})\}_{i=1}^{N_p}$ denote basis functions for P^N . We define the quadrature-based interpolation matrices $\mathbf{V}_q, \mathbf{V}_f$, mass matrix \mathbf{M} , and integrated differentiation matrices $\widehat{\mathbf{Q}}^i$

$$\begin{aligned} (\mathbf{V}_q)_{ij} &= \phi_j(\mathbf{x}_i), & (\mathbf{V}_f)_{ij} &= \phi_j(\mathbf{x}_i^f), \\ \mathbf{M} &= \mathbf{V}_q^T \mathbf{W} \mathbf{V}_q, & \mathbf{W} &= \text{diag}(\mathbf{w}), & (\widehat{\mathbf{Q}}_i)_{jk} &= \int_{\widehat{D}} \frac{\partial \phi_k}{\partial \widehat{x}_i} \phi_j. \end{aligned}$$

Finally, we introduce inner product notation on an element D^k

$$(u, v)_{D^k} = \int_{D^k} u(\mathbf{x})v(\mathbf{x}) \, dx, \quad \langle u, v \rangle_{\partial D^k} = \int_{\partial D^k} u(\mathbf{x})v(\mathbf{x}) \, dx$$

as well as over the entire domain Ω and its boundary $\partial\Omega$

$$(u, v)_\Omega = \sum_k (u, v)_{D^k}, \quad \langle u, v \rangle_{\partial\Omega} = \sum_k \langle u, v \rangle_{\partial D^k \cap \partial\Omega}.$$

In all numerical experiments, integrals are computed via quadrature approximations, which in turn induces discrete L^2 inner products which approximate continuous L^2 inner products over $D^k, \partial D^k$. Because the following proofs only use properties of quadrature-based L^2 inner products and do not assume exact integration, all theoretical results also hold under inexact quadrature.

3.3. Discretization of inviscid terms

For most numerical methods, the continuous identity (9) for the inviscid fluxes does not hold at the semi-discrete level. To address this issue, the inviscid terms are discretized using a “flux differencing” approach involving summation-by-parts (SBP) operators and entropy conservative fluxes [29]. We briefly review the construction of entropy stable methods for the inviscid case.

We introduce the quadrature-based projection matrix $\mathbf{P}_q = \mathbf{M}^{-1} \mathbf{V}_q^T \mathbf{W}$. Using \mathbf{P}_q and $\widehat{\mathbf{Q}}_i$, we can construct quadrature-based differentiation and extrapolation matrices \mathbf{Q}^i, \mathbf{E}

$$\mathbf{Q}_i = \mathbf{P}_q^T \widehat{\mathbf{Q}}_i \mathbf{P}_q, \quad \mathbf{E} = \mathbf{V}_f \mathbf{P}_q.$$

To accommodate general quadrature rules (e.g., both with and without boundary points), we introduce hybridized SBP operators. Let

$$\mathbf{B}_i = \text{diag}(\mathbf{w}_f \circ \widehat{\mathbf{n}}_i), \quad \mathbf{W}_f = \text{diag}(\mathbf{w}_f),$$

where \mathbf{w}_f is a vector of face quadrature points and $\widehat{\mathbf{n}}_i$ is a vector containing values of the i th scaled normal component $\widehat{n}_i \widehat{J}_f$ at surface quadrature points. Then, the hybridized SBP operator $\mathbf{Q}_{i,h}$ on the reference element \widehat{D} is defined as

$$\mathbf{Q}_{i,h} = \frac{1}{2} \begin{bmatrix} \mathbf{Q}_i - (\mathbf{Q}_i)^T & \mathbf{E}^T \mathbf{B}_i \\ \mathbf{B}_i \mathbf{E} & \mathbf{B}_i \end{bmatrix}.$$

We can construct operators $\mathbf{Q}_{i,h}^k$ on each physical element D^k as follows

$$\mathbf{Q}_{i,h}^k = \sum_{j=1}^d \mathbf{G}_{ij}^k \mathbf{Q}_{j,h},$$

where \mathbf{G}_{ij}^k are diagonal matrices containing the scaled geometric terms $J \frac{\partial \widehat{x}_j}{\partial x_i}$. Here, \widehat{x}_j and x_i denote the j th and i th reference and physical coordinates (14). We also introduce physical boundary matrices

$$\mathbf{B}_i^k = \mathbf{W}_f \text{diag}(\mathbf{n}_i \circ \mathbf{J}_f^k),$$

where $\mathbf{n}_i, \mathbf{J}_f^k$ are vectors containing values of n_i and J_f^k at surface quadrature points.

We now introduce entropy conservative numerical fluxes $\mathbf{f}_{i,S}(\mathbf{u}_L, \mathbf{u}_R)$ [29], which are bivariate functions of “left” and “right” states $\mathbf{u}_L, \mathbf{u}_R$. In addition to being symmetric and consistent, entropy conservative numerical fluxes satisfy an “entropy conservation” property

$$(\mathbf{v}_L - \mathbf{v}_R)^T \mathbf{f}_{i,S}(\mathbf{u}_L, \mathbf{u}_R) = \psi_i(\mathbf{u}_L) - \psi_i(\mathbf{u}_R). \quad (15)$$

The inviscid flux derivatives are approximated using a “flux differencing” approach. We first introduce the L^2 projection of the entropy variables and the “entropy projected” conservative variables $\widetilde{\mathbf{u}}$

$$\mathbf{v} = \mathbf{P}_q \mathbf{v}(\mathbf{V}_q \mathbf{u}), \quad \widetilde{\mathbf{u}} = \mathbf{u}(\mathbf{V}_h \mathbf{v}),$$

which are defined by evaluating the mapping from entropy to conservative variables using the projected entropy variables. Note that the projected entropy variables \mathbf{v} is a vector corresponding to modal coefficients, while $\widetilde{\mathbf{u}}$ corresponds to point values at volume and face quadrature points.

Then, $\frac{\partial \mathbf{f}_i(\mathbf{u})}{\partial x_i}$ on an element D^k is discretized by

$$\frac{\partial \mathbf{f}_i(\mathbf{u})}{\partial x_i} \iff \mathbf{V}_h^T \left(2\mathbf{Q}_{i,h}^k \circ \mathbf{F}_i \right) \mathbf{1}, \quad (\mathbf{F}_i)_{jk} = \mathbf{f}_{i,S}(\mathbf{u}_i, \mathbf{u}_j).$$

where \circ denotes the matrix Hadamard product. Since the entries of \mathbf{F}_i are vector-valued, the Hadamard product $\left(2\mathbf{Q}_{i,h}^k \circ \mathbf{F}_i \right)$ should be understood as each scalar entry of $2\mathbf{Q}_{i,h}^k$ multiplying each component of each vector-valued entry of \mathbf{F}_i .

Finally, let $\tilde{\mathbf{u}}^+$ denote the values of $\tilde{\mathbf{u}}$ on a neighboring element $D^{k,+}$. The inviscid discretization is completed by specifying interface fluxes which couple neighboring elements together, such that an entropy stable inviscid scheme over each element D^k is

$$\mathbf{M} \frac{d\mathbf{u}}{dt} + \sum_{i=1}^d \left[\mathbf{V}_h^T \left(2\mathbf{Q}_{i,h}^k \circ \mathbf{F}_i \right) \mathbf{1} + \mathbf{V}_f^T \left(\mathbf{B}_i^k \left(\mathbf{f}_{i,S} \left(\tilde{\mathbf{u}}^+, \tilde{\mathbf{u}} \right) - \mathbf{f}_i(\mathbf{u}) \right) \right) \right] - \mathbf{V}_f^T \mathbf{W}_f \frac{\lambda}{2} \llbracket \tilde{\mathbf{u}} \rrbracket = 0.$$

Here, we have added a simple entropy dissipative Lax-Friedrichs penalization term, where λ is the maximum of the wavespeed between the exterior and interior solution states $\tilde{\mathbf{u}}^+$ and $\tilde{\mathbf{u}}$. Other penalization terms such as HLLC and certain matrix penalizations [6, 30] also dissipate entropy.

All that remains for the implementation of the scheme is to specify the entropy conservative numerical fluxes $\mathbf{f}_S(\mathbf{u}_L, \mathbf{u}_R)$. All experiments in this paper utilize the entropy conservative and kinetic energy preserving numerical fluxes of Chandrashekar [31]. These fluxes utilize the logarithmic mean, which is computed in a numerically stable manner using the expansion derived in [32].

Remark 1. *While we have presented entropy stable DG schemes using a general “modal” DG framework, the formulation reduces to existing methods under appropriate choices of quadrature and basis. For example, specifying Gauss-Lobatto quadrature on a tensor product element recovers entropy stable spectral collocation schemes [15]. SBP discretizations without an underlying basis on simplices [10, 6, 7] can also be recovered for appropriate quadrature rules by setting $\mathbf{V}_q \mathbf{P}_q = \mathbf{I}$ [33].*

3.3.1. Entropy stable imposition of inviscid wall conditions

In the inviscid case, no-slip (no normal flow) boundary conditions are imposed at solid walls [22, 6]. These boundary conditions are consistent with all wall boundary conditions considered in this paper, and are imposed by enforcing

$$\rho^+ = \rho, \quad u_n^+ = -u_n, \quad u_\tau = u_\tau, \quad p^+ = p. \quad (16)$$

where u_n, u_τ denote the normal and tangential components of the velocity. Explicit expressions for u_n, u_τ in 2D are given by

$$\begin{aligned} u_n &= u_1 n_1 + u_2 n_2 \\ u_\tau &= u_1 n_2 - u_2 n_1. \end{aligned}$$

It was shown in [22, 6] that boundary contributions to the entropy balance equation (13) vanish under the imposition of reflective boundary conditions (??). For the remainder of this paper, we will assume that all viscous wall boundary conditions are paired with (and consistent with) these inviscid wall conditions.

3.4. Discretization of viscous terms

We discretize the symmetrized viscous terms (8) using a local DG formulation [34, 35], which is similar to the formulations introduced for nonlinear elliptic PDEs in [36]. We note that, while we presented the inviscid discretization using matrix notation, we utilize a variational formulation more familiar to finite element methods to describe the discretization of the viscous terms.

We begin by introducing Θ , which are DG approximations of the gradients of the entropy variables. Let $\mathbf{w}_{1,i} \in [P^N(\widehat{D})]^4$ denote vector-valued test functions for $i = 1, \dots, d$. The variational definition of Θ is then given by

$$(\Theta_i, \mathbf{w}_{1,i})_{D^k} = \left(\frac{\partial \mathbf{v}}{\partial x_i}, \mathbf{w}_{1,i} \right)_{D^k} + \frac{1}{2} \langle \llbracket \mathbf{v} \rrbracket n_i, \mathbf{w}_{1,i} \rangle_{\partial D^k}, \quad i = 1, \dots, d. \quad (17)$$

The terms Θ_1, Θ_2 are approximations of derivatives with respect to x_1, x_2 of the entropy variables \mathbf{v}_i . In the next step, we compute σ_i as the L^2 projection of $\sum_{j=1}^d \mathbf{K}_{ij} \Theta_j$ for $i = 1, 2$ onto the approximation space of each element

$$(\sigma_i, \mathbf{w}_{2,i})_{D^k} = \left(\sum_{j=1}^d \mathbf{K}_{ij} \Theta_j, \mathbf{w}_{2,i} \right)_{D^k}, \quad i = 1, \dots, d \quad (18)$$

for all $\mathbf{w}_{2,i} \in [P^N(\widehat{D})]^4$. Note that σ_i is an approximation to the viscous flux functions \mathbf{g}_i in the compressible Navier-Stokes equations (1) and (2).

We can now approximate the divergence of σ via \mathbf{g}_{visc} . Let τ_{visc} be a positive semi-definite penalty matrix which is single-valued over each element interface, which we will specify later. Then, the divergence of the viscous fluxes is approximated by \mathbf{g}_{visc} as

$$(\mathbf{g}_{\text{visc}}, \mathbf{w}_3)_{D^k} = \sum_{i=1}^d \left[\left(-\sigma_i, \frac{\partial \mathbf{w}_3}{\partial x_i} \right)_{D^k} + \langle \{\{\sigma_i\}\} n_i, \mathbf{w}_3 \rangle_{\partial D^k} \right] - \langle \tau_{\text{visc}} \llbracket \mathbf{v} \rrbracket, \mathbf{w}_3 \rangle_{\partial D^k}, \quad (19)$$

for $i = 1, \dots, d$ and for all $\mathbf{w}_3 \in [P^N(\widehat{D})]^4$. This approximation can be shown to be positive semi-definite in the following sense

Lemma 3.1. *Let \mathbf{g}_{visc} be defined by (17), (18), and (19). For periodic boundary conditions, the viscous entropy dissipation satisfies $(\mathbf{g}_{\text{visc}}, \mathbf{v}) \leq 0$.*

Proof. The proof is similar to those of [36, 37, 35]. Let $\mathbf{w}_3 = \mathbf{v}$, $\mathbf{w}_{1,i} = \sigma_i$, and $\mathbf{w}_2 = \theta$. Then, summing up (17), (18) and using (19) yield

$$\begin{aligned} (\mathbf{g}_{\text{visc}}, \mathbf{v})_{D^k} &= \sum_{i=1}^d \left[\left(-\sigma_i, \frac{\partial \mathbf{v}}{\partial x_i} \right)_{D^k} + \langle \{\{\sigma_i\}\} n_i, \mathbf{v} \rangle_{\partial D^k} \right] + \langle \tau_{\text{visc}} \llbracket \mathbf{v} \rrbracket, \mathbf{v} \rangle_{\partial D^k} \\ \sum_{i=1}^d (\Theta_i, \sigma_i)_{D^k} &= \sum_{i=1}^d \left(\frac{\partial \mathbf{v}}{\partial x_i}, \sigma_i \right)_{D^k} + \frac{1}{2} \langle \llbracket \mathbf{v} \rrbracket n_i, \sigma_i \rangle_{\partial D^k}, \\ \sum_{i=1}^d (\sigma_i, \Theta_i)_{D^k} &= \sum_{j=1}^d (\mathbf{K}_{ij} \Theta_j, \Theta_i)_{D^k}. \end{aligned}$$

We sum over all elements D^k , substitute the second equation into the first one, and use the third equation to yield

$$(\mathbf{g}_{\text{visc}}, \mathbf{v})_{D^k} = \sum_{i,j=1}^d \left[-(\mathbf{K}_{ij} \boldsymbol{\Theta}_j, \boldsymbol{\Theta}_i)_{D^k} + \frac{1}{2} \langle \llbracket \mathbf{v} \rrbracket n_j, \boldsymbol{\sigma}_j \rangle_{\partial D^k} + \langle \{\{\boldsymbol{\sigma}_j\}\} n_j, \mathbf{v} \rangle_{\partial D^k} \right] + \langle \boldsymbol{\tau}_{\text{visc}} \llbracket \mathbf{v} \rrbracket, \mathbf{v} \rangle_{\partial D^k}. \quad (20)$$

What remains is to show that the surface terms vanish when summed up over all elements. For periodic boundary conditions, all faces are ‘‘interior’’ faces shared by two elements. We split contributions from each surface term and swap them between D^k and the neighboring element $D^{k,+}$, such that

$$\begin{aligned} \sum_k \frac{1}{2} \langle \llbracket \mathbf{v} \rrbracket n_i, \boldsymbol{\sigma}_i \rangle_{\partial D^k} &= \frac{1}{2} \sum_k \left(\frac{1}{2} \langle \llbracket \mathbf{v} \rrbracket n_i, \boldsymbol{\sigma}_i \rangle_{\partial D^k} + \frac{1}{2} \langle \llbracket \mathbf{v} \rrbracket n_i, \boldsymbol{\sigma}_i^+ \rangle_{\partial D^{k,+}} \right) = \frac{1}{2} \sum_k \langle \llbracket \mathbf{v} \rrbracket n_i, \{\{\boldsymbol{\sigma}_i\}\} \rangle_{\partial D^k} \\ \sum_k \langle \{\{\boldsymbol{\sigma}_i\}\} n_i, \mathbf{v} \rangle_{\partial D^k} &= \frac{1}{2} \sum_k \left(\langle \{\{\boldsymbol{\sigma}_i\}\} n_i, \mathbf{v} \rangle_{\partial D^k} - \langle \{\{\boldsymbol{\sigma}_i\}\} n_i, \mathbf{v}^+ \rangle_{\partial D^{k,+}} \right) = -\frac{1}{2} \sum_k \langle \{\{\boldsymbol{\sigma}_i\}\} n_i, \llbracket \mathbf{v} \rrbracket \rangle_{\partial D^k} \\ \sum_k \langle \boldsymbol{\tau}_{\text{visc}} \llbracket \mathbf{v} \rrbracket, \mathbf{v} \rangle_{\partial D^k} &= \frac{1}{2} \sum_k \left(\langle \boldsymbol{\tau}_{\text{visc}} \llbracket \mathbf{v} \rrbracket, \mathbf{v} \rangle_{\partial D^k} - \langle \boldsymbol{\tau}_{\text{visc}} \llbracket \mathbf{v} \rrbracket, \mathbf{v}^+ \rangle_{\partial D^{k,+}} \right) = -\frac{1}{2} \langle \boldsymbol{\tau}_{\text{visc}} \llbracket \mathbf{v} \rrbracket, \llbracket \mathbf{v} \rrbracket \rangle_{\partial D^k} \end{aligned}$$

Here, we have used that both n_i and $\llbracket \mathbf{v} \rrbracket$ change sign between D^k and $D^{k,+}$. Thus, the surface terms cancel, and by the positive semi-definiteness of \mathbf{K}_{ij} ,

$$\sum_k (\mathbf{g}_{\text{visc}}, \mathbf{v})_{D^k} = \sum_k \sum_{i,j=1}^d -(\mathbf{K}_{ij} \boldsymbol{\Theta}_j, \boldsymbol{\Theta}_i)_{D^k} - \frac{1}{2} \langle \boldsymbol{\tau}_{\text{visc}} \llbracket \mathbf{v} \rrbracket, \llbracket \mathbf{v} \rrbracket \rangle_{\partial D^k} \leq 0$$

since $\boldsymbol{\tau}_{\text{visc}}$ is a positive semi-definite matrix. \square

Remark 2. *This proof uses only properties of L^2 inner products, which are preserved if all inner products and integrals are computed using quadrature. The negative semi-definite structure is also preserved on curved meshes with spatially varying geometric terms if either an SBP property holds or if the derivative lies on the test function in (17) and the derivative lies on $\boldsymbol{\sigma}_i$ in (19). In the former case, the extension to curved meshes is essentially the same as in [38], while for the latter case the treatment of viscous terms resembles that of the ‘‘strong-weak’’ formulation for DG discretizations of symmetric wave equations [39].*

4. Entropy stable imposition of wall boundary conditions

We now turn our focus to the entropy stable imposition of adiabatic and isothermal no-slip wall boundary conditions for the compressible Navier-Stokes equations, as well as the entropy stable treatment of slip boundary conditions. Boundary conditions are imposed by choosing appropriate exterior states $\tilde{\mathbf{u}}^+, \mathbf{v}^+$ such that the contributions from the boundary terms in the proof of Lemma 3.1 reduce to appropriate quantities [40, 41, 42].

Let $\langle u, v \rangle_{\partial \Omega} = \int_{\partial \Omega} uv$ denote the inner product on the domain boundary $\partial \Omega$. For the following proofs we will assume that $\boldsymbol{\tau}_{\text{visc}} = 0$ on $\partial \Omega$, and postpone the discussion of entropy-dissipative

boundary penalization matrices to Section 4.4. Then, the total viscous entropy contribution is

$$\sum_k (\mathbf{g}_{\text{visc}}, \mathbf{v})_{D^k} = \left(\sum_k \sum_{i,j=1}^d -(\mathbf{K}_{ij} \boldsymbol{\Theta}_j, \boldsymbol{\Theta}_i)_{D^k} \right) + \sum_{i=1}^d \left[\frac{1}{2} \langle [\mathbf{v}] n_i, \boldsymbol{\sigma}_i \rangle_{\partial\Omega} + \langle \{\{\boldsymbol{\sigma}_i\}\} n_i, \mathbf{v} \rangle_{\partial\Omega} \right]. \quad (21)$$

Our goal will be to construct exterior states for which the discrete viscous entropy-dissipative terms (21) mimic the continuous viscous entropy dissipative terms in (12).

In the following sections, , we will refer to individual components of the viscous fluxes $\boldsymbol{\sigma}_i$ by

$$(\boldsymbol{\sigma}_i)_j = \sigma_{j,i}, \quad j = 1, \dots, d,$$

for consistency with the $\tau_{i,j}$ notation in (3). We will also restrict ourselves to the two-dimensional case $d = 2$ for simplicity of presentation. Recall that the conservative variables are ρ, u_1, u_2, E , and the entropy variables correspond to

$$v_1 = \frac{\rho e (\gamma + 1 - s) - E}{\rho e}, \quad v_2 = \frac{\rho u_1}{\rho e}, \quad v_3 = \frac{\rho u_2}{\rho e}, \quad v_4 = -\frac{\rho}{\rho e}.$$

The extension to $d = 3$ involves straightforward modifications to account for the z -component of the normal vector and velocity vector.

4.1. Adiabatic no-slip wall boundary conditions

Adiabatic no-slip wall conditions impose zero normal velocity conditions, velocity conditions, and an ‘‘entropy flow’’ condition on the temperature gradient through the wall

$$u_n = 0, \quad \mathbf{u}_\tau = \mathbf{u}_{\text{wall}}, \quad \kappa \frac{\partial T}{\partial n} = g(t).$$

where $u_n = u_1 n_1 + u_2 n_2$ and $u_\tau = u_1 n_2 - u_2 n_1$ in 2D. For simplicity of notation, we will convert boundary conditions on normal and tangential components to boundary conditions on velocity in each coordinate direction

$$u_i = u_{i,\text{wall}}, \quad i = 1, \dots, d.$$

The terms which naturally appear in the DG formulation involve only traces of entropy variables and approximations of the viscous fluxes. However, we can impose no-slip velocity conditions by noting that the entropy variables v_2, \dots, v_{1+d} in (7) are the components of the velocity u_i scaled by e^{-1} , and that $v_4 = -1/e$. Then, the velocity boundary conditions can equivalently be imposed as

$$v_{1+i} = \frac{u_{i,\text{wall}}}{e} = -u_{i,\text{wall}} v_4, \quad i = 1, \dots, d.$$

We impose these conditions by specifying the exterior states

$$v_{1+i}^+ = -2u_{i,\text{wall}} v_4 - v_{1+i}, \quad i = 1, \dots, d \quad (22)$$

such that $\{\{v_{1+i}\}\} = u_{i,\text{wall}} v_4$.

We now consider the adiabatic wall condition. Note that the variables $\boldsymbol{\sigma}_i$ in (18) are approximations to the viscous fluxes \mathbf{g}_i in (2), which include the heat flux in the last component of \mathbf{g}_i . In

two dimensions, the definitions of $\sigma_{i,j}$ correspond to

$$\begin{aligned}\sigma_{2,i} &= \tau_{1,i} \\ \sigma_{3,i} &= \tau_{2,i} \\ \sigma_{4,i} &= \tau_{1,i}u_1 + \tau_{2,i}u_2 - \kappa \frac{\partial T}{\partial x_i}, \quad i = 1, \dots, 2.\end{aligned}$$

We impose adiabatic wall boundary conditions for by specifying $\sigma_{4,i}^+$ as

$$\sigma_{4,i}^+ = 2 \left(u_{1,\text{wall}}\sigma_{2,i} + u_{2,\text{wall}}\sigma_{3,i} + \frac{c_v g(t)n_i}{v_4} \right) - \sigma_{4,i}, \quad (23)$$

such that the average of $\sigma_{4,i}$ incorporates wall velocities and heat entropy flow into the formula for the viscous energy flux

$$\{\{\sigma_{4,i}\}\} = u_{1,\text{wall}}\sigma_{2,i} + u_{2,\text{wall}}\sigma_{3,i} + \frac{c_v g(t)n_i}{v_4}.$$

Finally, since no boundary conditions are imposed on $\sigma_{2,i}$, $\sigma_{3,i}$, and v_4 , we simply set the exterior values equal to the interior values for $i = 1, 2$

$$\sigma_{2,i}^+ = \sigma_{2,i}, \quad \sigma_{3,i}^+ = \sigma_{3,i}, \quad v_4^+ = v_4 \quad (24)$$

such that the average quantities are $\{\{\sigma_{j,i}\}\} = \sigma_{j,i}$ for $j = 2, 3$ and $\{\{v_4\}\} = v_4$. Note that \mathbf{v}_1^+ can be arbitrarily chosen since $\sigma_{1,i} = 0$ due to the fact that the corresponding rows of \mathbf{K}_{ij} are zero. Based on these exterior states, we have the following theorem:

Theorem 4.1. *Let \mathbf{g}_{visc} denote viscous contributions from (17), (18), and (19). If adiabatic no-slip wall boundary conditions are imposed using exterior states for $i = 1, \dots, d$ in $d = 2$ dimensions*

$$\begin{aligned}v_{1+i}^+ &= -2u_{i,\text{wall}}v_4 - v_{1+i} \\ v_4^+ &= v_4 \\ \sigma_{2,i}^+ &= \sigma_{2,i}, \\ \sigma_{3,i}^+ &= \sigma_{3,i}, \\ \sigma_{4,i}^+ &= 2 \left(u_{1,\text{wall}}\sigma_{2,i} + u_{2,\text{wall}}\sigma_{3,i} + \frac{c_v g(t)n_i}{v_4} \right) - \sigma_{4,i},\end{aligned}$$

then the viscous contribution \mathbf{g}_{visc} mimics the entropy balance such that

$$\sum_k (\mathbf{g}_{\text{visc}}, \mathbf{v})_{D^k} = \sum_{i=1}^d \langle c_v g(t), 1 \rangle_{\partial\Omega} - \sum_k \left(\sum_{i,j=1}^d (\mathbf{K}_{ij} \boldsymbol{\Theta}_j, \boldsymbol{\Theta}_i)_{D^k} \right).$$

Proof. Plugging the exterior values into the boundary terms in (21) simplify to

$$\begin{aligned}
\sum_{i=1}^d \left[\frac{1}{2} \langle \llbracket \mathbf{v} \rrbracket n_i, \boldsymbol{\sigma}_i \rangle_{\partial\Omega} + \langle \{\{\boldsymbol{\sigma}_i\}\} n_i, \mathbf{v} \rangle_{\partial\Omega} \right] &= \sum_{i=1}^d \langle -u_{1,\text{wall}}v_4 - v_2, \sigma_{2,i}n_i \rangle_{\partial\Omega} + \langle \sigma_{2,i}n_i, v_2 \rangle_{\partial\Omega} \\
&+ \sum_{i=1}^d \langle -u_{2,\text{wall}}v_4 - v_3, \sigma_{3,i}n_i \rangle_{\partial\Omega} + \langle \sigma_{3,i}n_i, v_3 \rangle_{\partial\Omega} \\
&+ \sum_{i=1}^d \left\langle u_{1,\text{wall}}\sigma_{2,i} + u_{2,\text{wall}}\sigma_{3,i} + \frac{c_v g(t)n_i}{v_4}, v_4 n_i \right\rangle_{\partial\Omega} \\
&= \langle c_v g(t), 1 \rangle_{\partial\Omega}.
\end{aligned}$$

□

As noted in [25], if $g(t) = 0$, then the boundary term resulting from Theorem 4.1 vanishes and the resulting discretization is entropy stable.

4.2. Isothermal no-slip wall conditions

Isothermal no-slip wall boundary conditions impose tangential wall velocity conditions and a fixed temperature at the wall

$$u_i = u_{i,\text{wall}}, \quad i = 1, \dots, d, \quad T = T_{\text{wall}}.$$

To impose $T = T_{\text{wall}}$, we use that $v_4 = -1/e = -1/(c_v T)$ and set the exterior state v_4^+ as

$$v_4^+ = -\frac{2}{c_v T_{\text{wall}}} - v_4, \quad \sigma_{4,i}^+ = \sigma_{4,i}, \quad i = 1, 2,$$

such that $\{\{v_4\}\} = -1/(c_v T_{\text{wall}})$ and $\{\{\sigma_{4,i}\}\} = \sigma_{4,i}$. We also incorporate T_{wall} into the exterior values v_2^+, v_3^+ . We have the following theorem on entropy stability of isothermal wall boundary conditions:

Theorem 4.2. *Let \mathbf{g}_{visc} denote viscous contributions from (17), (18), and (19). If isothermal no-slip wall boundary conditions are imposed by setting the exterior states for $i = 1, \dots, d$ in $d = 2$ dimensions*

$$\begin{aligned}
v_{1+i}^+ &= \frac{2u_{i,\text{wall}}}{c_v T_{\text{wall}}} - v_{1+i} \\
v_4^+ &= -\frac{2}{c_v T_{\text{wall}}} - v_4 \\
\sigma_{2,i}^+ &= \sigma_{2,i}, \\
\sigma_{3,i}^+ &= \sigma_{3,i}, \\
\sigma_{4,i}^+ &= \sigma_{4,i},
\end{aligned}$$

then the viscous contribution \mathbf{g}_{visc} mimics the entropy balance such that

$$\sum_k (\mathbf{g}_{\text{visc}}, \mathbf{v})_{D^k} = \sum_{i=1}^d \left\langle \frac{q_n}{c_v T_{\text{wall}}}, 1 \right\rangle_{\partial\Omega} - \sum_k \left(\sum_{i,j=1}^d (\mathbf{K}_{ij} \boldsymbol{\Theta}_j, \boldsymbol{\Theta}_i)_{D^k} \right).$$

Here, we have introduced the normal heat flux $q_n = \sum_{i=1}^d q_i n_i$, where q_i is defined as

$$q_i = -\sigma_{4,i} + u_{1,\text{wall}}\sigma_{2,i} + u_{2,\text{wall}}\sigma_{3,i} \approx -\kappa \frac{\partial T}{\partial x_i}.$$

Proof. Under this choice of exterior states, the boundary terms in (21) simplify to

$$\begin{aligned} \sum_{i=1}^d \left[\frac{1}{2} \langle \llbracket \mathbf{v} \rrbracket n_i, \boldsymbol{\sigma}_i n_i \rangle_{\partial\Omega} + \langle \{\{\boldsymbol{\sigma}_i\}\} n_i, \mathbf{v} \rangle_{\partial\Omega} \right] &= \sum_{i=1}^d \left\langle \frac{u_{1,\text{wall}}}{c_v T_{\text{wall}}} - v_2, \sigma_{2,i} n_i \right\rangle_{\partial\Omega} + \langle \sigma_{2,i} n_i, v_2 \rangle_{\partial\Omega} \\ &+ \sum_{i=1}^d \left\langle \frac{u_{2,\text{wall}}}{c_v T_{\text{wall}}} - v_3, \sigma_{3,i} n_i \right\rangle_{\partial\Omega} + \langle \sigma_{3,i} n_i, v_3 \rangle_{\partial\Omega} \\ &+ \sum_{i=1}^d \left\langle -\frac{1}{c_v T_{\text{wall}}} - v_4, \sigma_{4,i} n_i \right\rangle_{\partial\Omega} + \langle \sigma_{4,i}, v_4 n_i \rangle_{\partial\Omega} \\ &= \sum_{i=1}^d \left\langle \underbrace{-\sigma_{4,i} + u_{1,\text{wall}}\sigma_{2,i} + u_{2,\text{wall}}\sigma_{3,i}}_{q_i}, \frac{1}{c_v T_{\text{wall}}} n_i \right\rangle_{\partial\Omega} \\ &= \left\langle \frac{q_n}{c_v T_{\text{wall}}}, 1 \right\rangle_{\partial\Omega}. \end{aligned}$$

□

Since the wall temperature T_{wall} is assumed to be positive, this boundary contribution does not vanish and the resulting discretization cannot be proven to be entropy stable. However, the boundary contribution mimics the boundary terms in the continuous entropy balance equation (12), which do not vanish at isothermal walls.

4.3. Reflective wall (symmetry) conditions

Finally, we consider reflective boundary conditions, which are the viscous extension of the reflective wall boundary conditions for the inviscid case of the compressible Euler equations [22, 6, 43]. In the context of viscous flows, these boundary conditions can be used to enforce symmetry conditions or free surfaces. Recall from Section 3.3.1 that inviscid reflective wall boundary conditions are enforced by setting exterior values for the convective flux

$$\rho^+ = \rho, \quad u_n^+ = -u_n, \quad u_\tau = u_\tau, \quad p^+ = p$$

We note that these conditions correspond to continuous boundary conditions on the normal velocity and normal heat flux

$$u_n = 0, \quad \kappa \frac{\partial T}{\partial n} = 0. \quad (25)$$

Let n_1, n_2 denote the components of the unit normal vector. The conditions on normal velocity imply that the velocity reduces to its tangential component. This is enforced by setting

$$u_i^+ = u_i - 2u_n n_i, \quad i = 2, \dots, d+1,$$

such that $\sum_{i=1}^d \{\{u_i\}\} n_i = 0$ and the normal component of the averaged velocity vanishes.

Since $e = c_v T > 0$ for $T > 0$, the second and third entropy variables $v_2, v_3 = u/e, v/e$ are well-defined. Thus, reflective wall boundary conditions are also equivalent to the following conditions on the second and third entropy variables

$$v_i^+ = v_i - 2v_n n_i, \quad (26)$$

where $v_n = v_2 n_1 + v_3 n_2$ in 2D.

We now consider viscous contributions. Note that $\{\{\sigma_{1,j}\}\} = 0$ since there is no mass diffusion, and terms involving σ_1 vanish. We thus begin by considering fields corresponding to $i = 2, 3$. Using (26), the boundary terms involving $\llbracket v_i \rrbracket$ for $i = 2, 3$ in (21) can be expanded out as

$$\sum_{i=1,2} \left\langle \frac{1}{2} \llbracket v_{1+i} \rrbracket, \sum_{j=1}^d \sigma_{1+i,j} n_j \right\rangle = \frac{1}{2} \left\langle v_n, \sum_{i,j=1}^d \sigma_{1+i,j} n_i n_j \right\rangle_{\partial\Omega} = \frac{1}{2} \left\langle v_2 n_1 + v_3 n_2, \sum_{i,j=1}^d \sigma_{1+i,j} n_i n_j \right\rangle_{\partial\Omega}.$$

We can write this in matrix form using the unit normal vector $\mathbf{n} = [n_1, n_2]^T$

$$\frac{1}{2} \left\langle v_2 n_1 + v_3 n_2, \sum_{i,j=1}^d \sigma_{1+i,j} n_i n_j \right\rangle = \frac{1}{2} \left\langle \begin{bmatrix} v_2 \\ v_3 \end{bmatrix} \cdot \mathbf{n}, \mathbf{n}^T \begin{bmatrix} \sigma_{2,1} & \sigma_{2,2} \\ \sigma_{3,1} & \sigma_{3,2} \end{bmatrix} \mathbf{n} \right\rangle_{\partial\Omega} \quad (27)$$

Recall that in 2D, the boundary contributions involving $\{\{\sigma_{i,j}\}\}$ are

$$\sum_{i=1,2} \left\langle \sum_{j=1}^d \{\{\sigma_{1+i,j}\}\} n_j, v_{1+i} \right\rangle_{\partial\Omega} = \frac{1}{2} \left\langle \begin{bmatrix} v_2 \\ v_3 \end{bmatrix}, \begin{bmatrix} \{\{\sigma_{2,1}\}\} & \{\{\sigma_{2,2}\}\} \\ \{\{\sigma_{3,1}\}\} & \{\{\sigma_{3,2}\}\} \end{bmatrix} \mathbf{n} \right\rangle_{\partial\Omega}.$$

These contributions will cancel with (27) if the tangential-normal component of the stress vanishes. This condition is equivalent to the stress on the boundary reducing to the normal-normal component

$$\begin{bmatrix} \{\{\sigma_{2,1}\}\} & \{\{\sigma_{2,2}\}\} \\ \{\{\sigma_{3,1}\}\} & \{\{\sigma_{3,2}\}\} \end{bmatrix} \mathbf{n} = \mathbf{n} \mathbf{n}^T \begin{bmatrix} \sigma_{2,1} & \sigma_{2,2} \\ \sigma_{3,1} & \sigma_{3,2} \end{bmatrix} \mathbf{n}.$$

This implies that $\{\{\sigma_{1+i,j}\}\}$ can be expressed in terms of the normal stress

$$\{\{\sigma_{1+i,j}\}\} = n_j \sigma_{n,j} \quad (28)$$

$$\sigma_{n,j} = \sum_{i=1}^d \sigma_{1+i,j} n_i, \quad i = 1, \dots, d. \quad (29)$$

Finally, we consider contributions involving v_4 and $\sigma_{4,i}$

$$\sum_{j=1}^d \langle \{\{\sigma_{4,j}\}\} n_j, v_4 \rangle_{\partial\Omega} + \left\langle \frac{1}{2} \llbracket v_4 \rrbracket, \sigma_{4,j} n_j \right\rangle_{\partial\Omega}. \quad (30)$$

Since $v_4 = -1/e$ and $\rho^+, p^+ = \rho, p$ from the inviscid wall boundary conditions, we set the exterior state $v_4^+ = v_4$. The remaining boundary term in (30) vanishes as well if also we impose $\sigma_{4,i}^+ = -\sigma_{4,i}$.

We note that this corresponds to a zero normal heat flux condition $\kappa \frac{\partial T}{\partial n} = 0$. Recall from (23) that $\sigma_{4,i}$ corresponds to $\sigma_{4,i} = u_1 \sigma_{2,i} + u_2 \sigma_{3,i} - \kappa \frac{\partial T}{\partial x_i}$, such that

$$\sum_{j=1}^d \sigma_{4,j} n_j = \left(\sum_{i,j=1}^d u_i \sigma_{i+1,j} n_j \right) - \kappa \frac{\partial T}{\partial n}.$$

Recall from (29) that the stress reduces to the normal-normal stress on the boundary. We rewrite this using the velocity vector $\mathbf{u} = [u_1, u_2]^T$ such that

$$\sum_{i,j=1}^d u_i \sigma_{i+1,j} n_j = \begin{bmatrix} u_1 \\ u_2 \end{bmatrix}^T \mathbf{n} \mathbf{n}^T \begin{bmatrix} \sigma_{2,1} & \sigma_{2,2} \\ \sigma_{3,1} & \sigma_{3,2} \end{bmatrix} \mathbf{n} = (\mathbf{u}^T \mathbf{n}) \left(\mathbf{n}^T \begin{bmatrix} \sigma_{2,1} & \sigma_{2,2} \\ \sigma_{3,1} & \sigma_{3,2} \end{bmatrix} \mathbf{n} \right) = 0$$

since $(\mathbf{u}^T \mathbf{n}) = u_n = 0$ by the reflective wall boundary condition (25). Thus, on reflective (symmetry) boundaries, the contributions involving $\sigma_{4,j}$ correspond to

$$\sum_{j=1}^d \sigma_{4,j} n_j = -\kappa \frac{\partial T}{\partial n}$$

such that $\sigma_{4,i}^+ = -\sigma_{4,i}$ imposes a zero adiabatic wall condition. We summarize this as follows:

Theorem 4.3. *Let \mathbf{g}_{visc} denote viscous contributions from (17), (18), and (19). Let v_n be analogous to the normal velocity, such that v_n and the normal stresses $\sigma_{n,j}$ are defined as*

$$v_n = \sum_{i=1}^d v_{1+i} n_i, \quad \sigma_{n,j} = \sum_{i=1}^d \sigma_{1+i,j} n_i, \quad i = 1, \dots, d.$$

In $d = 2$ dimensions, if reflective (symmetry) boundary conditions are imposed by setting the exterior states for $i = 1, \dots, d$

$$\begin{aligned} v_{1+i}^+ &= v_{1+i} - 2v_n n_i \\ v_4^+ &= v_4 \\ \sigma_{1+i,j}^+ &= 2n_i \sigma_{n,j} - \sigma_{1+i,j} \\ \sigma_{4,i}^+ &= -\sigma_{4,i}, \end{aligned}$$

then the viscous contribution \mathbf{g}_{visc} mimics the entropy balance such that

$$\sum_k (\mathbf{g}_{\text{visc}}, \mathbf{v})_{D^k} = - \sum_k \left(\sum_{i,j=1}^d (\mathbf{K}_{ij} \Theta_j, \Theta_i)_{D^k} \right).$$

Moreover, these exterior states correspond to imposing zero normal flow, zero tangential-normal stress, and zero adiabatic wall conditions.

4.4. Entropy dissipative boundary penalization matrices

Since boundary conditions are imposed weakly, it can be useful to penalize the deviation of the solution from the boundary data. To do so, we modify the penalization matrix $\boldsymbol{\tau}_{\text{visc}}$ on boundary faces. The resulting matrix is non-symmetric on boundary faces in order to account for the fact that $\boldsymbol{\tau}_{\text{visc}}$ now only incorporates contributions from one element, as opposed to interior interfaces which include contributions from both an element and its neighbor.

Let $\boldsymbol{\tau}_{\text{visc}}$ be defined on boundary faces as

$$\boldsymbol{\tau}_{\text{visc}} = \tau \begin{bmatrix} 0 & & & \\ & -1 & & \\ & & -1 & \\ \frac{\{\{v_2\}\}}{v_4} & \frac{\{\{v_3\}\}}{v_4} & \frac{\llbracket v_4 \rrbracket}{2v_4} & \end{bmatrix} \quad (31)$$

where $\tau \geq 0$ is a scalar penalization parameter.

Note that division by v_4 is well-defined if the temperature $T > 0$ since $v_4 = -1/T < 0$. We then have the following result:

Theorem 4.4. *Let $\boldsymbol{\tau}_{\text{visc}}$ be given by (31). Then, the penalty term is entropy dissipative in that*

$$-\langle \boldsymbol{\tau}_{\text{visc}} \llbracket \mathbf{v} \rrbracket, \mathbf{v} \rangle_{\partial\Omega} = -\frac{\tau}{2} (\langle \llbracket v_2 \rrbracket, \llbracket v_2 \rrbracket \rangle_{\partial\Omega} + \langle \llbracket v_3 \rrbracket, \llbracket v_3 \rrbracket \rangle_{\partial\Omega} + \langle \llbracket v_4 \rrbracket, \llbracket v_4 \rrbracket \rangle_{\partial\Omega}) \leq 0.$$

Proof. Plugging in the values for v_2^+, v_3^+, v_4^+ , the penalty term reduces to

$$-\langle \boldsymbol{\tau}_{\text{visc}} \llbracket \mathbf{v} \rrbracket, \mathbf{v} \rangle_{\partial\Omega} = -\tau (\langle -\llbracket v_2 \rrbracket, v_2 \rangle_{\partial\Omega} + \langle -\llbracket v_3 \rrbracket, v_3 \rangle_{\partial\Omega}) \quad (32)$$

$$- \tau \left\langle \llbracket v_2 \rrbracket \frac{\{\{v_2\}\}}{v_4} + \llbracket v_3 \rrbracket \frac{\{\{v_3\}\}}{v_4}, v_4 \right\rangle_{\partial\Omega} \quad (33)$$

$$- \tau \left\langle \frac{\llbracket v_4 \rrbracket}{v_4} \llbracket v_4 \rrbracket, v_4 \right\rangle_{\partial\Omega}$$

Omitting τ for now, the final term reduces to $\left\langle \frac{\llbracket v_4 \rrbracket}{2v_4} \llbracket v_4 \rrbracket, v_4 \right\rangle_{\partial\Omega} = \frac{1}{2} \langle \llbracket v_4 \rrbracket, \llbracket v_4 \rrbracket \rangle_{\partial\Omega}$, while the third term reduces to

$$\left\langle \llbracket v_2 \rrbracket \frac{\{\{v_2\}\}}{v_4} + \llbracket v_3 \rrbracket \frac{\{\{v_3\}\}}{v_4}, v_4 \right\rangle_{\partial\Omega} = \langle \llbracket v_2 \rrbracket, \{\{v_2\}\} \rangle + \langle \llbracket v_3 \rrbracket, \{\{v_3\}\} \rangle_{\partial\Omega}.$$

Using this, adding together (32) and (33) then yields

$$\begin{aligned} \langle \boldsymbol{\tau}_{\text{visc}} \llbracket \mathbf{v} \rrbracket, \mathbf{v} \rangle_{\partial\Omega} &= -\tau [\langle \llbracket v_2 \rrbracket, \{\{v_2\}\} - v_2 \rangle_{\partial\Omega} + \langle \llbracket v_3 \rrbracket, \{\{v_3\}\} - v_3 \rangle_{\partial\Omega}] \\ &= -\frac{\tau}{2} [\langle \llbracket v_2 \rrbracket, \llbracket v_2 \rrbracket \rangle_{\partial\Omega} + \langle \llbracket v_3 \rrbracket, \llbracket v_3 \rrbracket \rangle_{\partial\Omega}]. \end{aligned}$$

□

Remark 3. *When imposing heat entropy flux wall boundary conditions in Theorem 4.1, $\llbracket v_4 \rrbracket = 0$ and no penalization is applied to the component $v_4 = -1/T$.*

Remark 4. *We can relate $\boldsymbol{\tau}_{\text{visc}}$ to the choice of penalty matrix in [25] if $\tau \propto -1/v_4 = e > 0$ and $\mu = 1, \lambda = 0$. For our numerical experiments, we choose $\tau = -\frac{1}{(\text{Re})v_4} > 0$, which mimics the scaling with respect to Reynolds number and T of the penalization introduced in [25]. However, a simpler choice of τ as an $O(1)$ constant does not produce significantly different results for the numerical experiments reported in this work.*

5. Numerical experiments

In this section, we present numerical experiments which verify the theoretical results proven in this work. All numerical experiments utilize the adaptive 5th order Dormand-Prince time integration [44] to advance the solution forward in time.

Unless specified otherwise, all numerical experiments utilize a Lax-Friedrichs penalization [6, 8], where the maximum wavespeed is estimated as the maximum of the wavespeeds evaluated at the left and right states [45]. For viscous interior dissipation, we simply take τ_{visc} to be

$$\tau_{\text{visc}} = \tau \begin{bmatrix} 0 & & \\ & \mathbf{I}_{(d+1) \times (d+1)} & \\ & & \end{bmatrix},$$

where τ is a scalar value as discussed in Remark 4. This results in an entropy dissipation which is proportional to the norms of $[[v_2]]$, $[[v_3]]$, $[[v_4]]$ over each element interface.

5.1. Verification of accuracy

We begin by testing convergence of the difference between the numerical solution and the imposed boundary conditions. Recall that for DG methods, the boundary conditions are imposed weakly, such that the solution does not satisfy the boundary conditions exactly. We examine convergence of the solution to zero wall boundary conditions for a simple periodic channel setup on $[-2, 2] \times [-1, 1]$. Periodic boundary conditions are imposed in the x direction and zero adiabatic wall boundary conditions are imposed on the top and bottom walls. Simulations are run until final time $T_{\text{final}} = .5$ and compute the L^2 error (in other words, the L^2 norm of the x and y velocities) for the initial conditions

$$\rho = 1, \quad u_1 = \frac{1}{10} \sin\left(\frac{\pi x}{2}\right) \cos\left(\frac{\pi y}{2}\right), \quad u_2 = \frac{1}{10} \cos\left(\frac{\pi x}{2}\right) \sin(\pi y), \quad p = \frac{1}{\text{Ma}^2 \gamma}.$$

We utilize $\text{Ma} = .1$ and $\text{Re} = 50$. The boundary penalization described in Theorem 4.4 is also applied. Each mesh is constructed by subdividing a quadrilateral mesh of $2K_{1D} \times K_{1D}$ elements to produce a triangular mesh. Moreover, to ensure that viscous effects near the boundary did not impact convergence, we utilized graded meshes constructed by transforming the y -coordinates a uniform triangular mesh via $\tilde{y} = y + .25 \sin(\pi y)$ (see Figure 1).

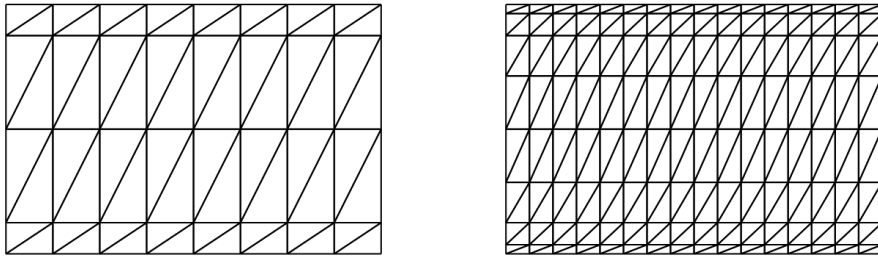


Figure 1: Examples of two meshes in the sequence of meshes used for the convergence study.

Table 1 shows computed errors $e_{\text{wall}} = \left(\int_{\partial\Omega_{\text{wall}}} u^2 + v^2 \right)^{1/2}$ for the velocity on the wall boundary $\partial\Omega_{\text{wall}}$ at $y = \pm 1$. We observe asymptotic convergence rates between $O(h^{N+1})$ and $O(h^{N+2})$. We

$K_{1D} \backslash N$	1	Rate	2	Rate	3	Rate	4	Rate
2	3.97e-4		4.68e-4		4.32e-4		4.56e-4	
4	3.45e-4	.205	5.31e-4	-.181	3.26e-4	.401	1.08e-4	2.08
8	3.20e-4	.106	7.30e-5	2.86	6.57e-6	5.63	6.29e-7	7.42
16	7.74e-5	2.05	5.35e-6	3.77	1.73e-7	5.25	1.71e-8	5.20

(a) Ma = .1

$K_{1D} \backslash N$	1	Rate	2	Rate	3	Rate	4	Rate
2	8.32e-3		1.16e-2		8.81e-3		4.88e-3	
4	6.95e-3	.256	2.19e-3	2.41	2.53e-4	5.12	1.21e-4	5.34
8	1.13e-3	2.63	6.18e-5	5.14	1.26e-5	4.32	1.55e-6	6.29
16	1.97e-4	2.52	4.67e-6	3.73	4.66e-7	4.76	2.23e-8	6.12

(b) Ma = .3

Table 1: L^2 errors for the imposition of no-slip velocity boundary conditions for Re = 50 at $T_{\text{final}} = 1/2$.

note that these rates are slightly higher than the optimal $O(h^{N+1})$ L^2 rate of convergence (which was observed in [23] for zero no-slip boundary conditions) due to the fact that the exact velocity is zero and is exactly representable by the DG approximation space. We also performed additional experiments which suggest that removing boundary penalization does not affect numerical behavior significantly, producing slightly larger errors on the coarsest meshes and roughly the same level of error on finer meshes.

5.2. Lid-driven cavity

We now test the imposition of viscous boundary conditions on the lid-driven cavity problem. This problem is typically used to benchmark incompressible fluid solvers [46], though numerical experiments have also been performed for compressible flows [47]. The domain is the bi-unit box $[-1, 1]^2$, and zero no-slip conditions are imposed on the left, right, and bottom boundaries. For all experiments, we take Ma = .1 and impose $u_1 = 1$ and $u_2 = 0$ on the top boundary. Initial conditions are set to be

$$\rho = 1, \quad u_1 = u_2 = 0, \quad p = \frac{1}{\text{Ma}^2 \gamma}.$$

We also augment the velocity boundary conditions with either adiabatic or isothermal temperature boundary conditions to test the new entropy stable wall boundary conditions derived in this work.

We first consider the imposition of adiabatic boundary conditions with $g(t) = 0$. All triangular meshes are constructed by bisecting a uniform quadrilateral mesh of $K_{1D} \times K_{1D}$ elements. Figure 2 shows the norm of the velocity at final time $T_{\text{final}} = 100$ for Re = 100, 1000, 10000. Simulations are performed using degree $N = 3$ polynomials and $K_{1D} = 16$. While most solution features for Re = 100, 1000 are well-resolved, we note that there is under-resolution near the top left and right hand corners of the domain. This is due to the fact that the velocity boundary conditions are discontinuous between the left and right walls and the lid. However, the simulation remains stable despite this under-resolution.

The solutions are similar to solutions found in the literature; however, our main goal is to verify the entropy balance results proven in Theorem 4.1. We solve the lid-driven cavity problem with

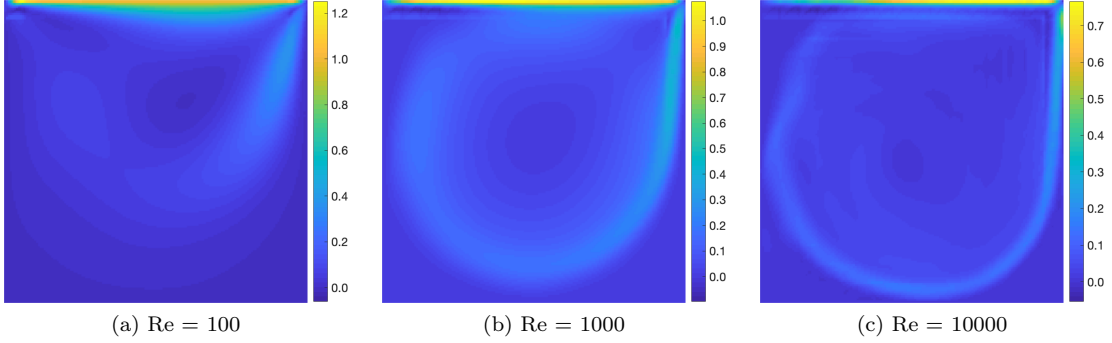


Figure 2: Norm of velocity for the lid-driven cavity problem for $Ma = .1$ and $T_{\text{final}} = 100$.

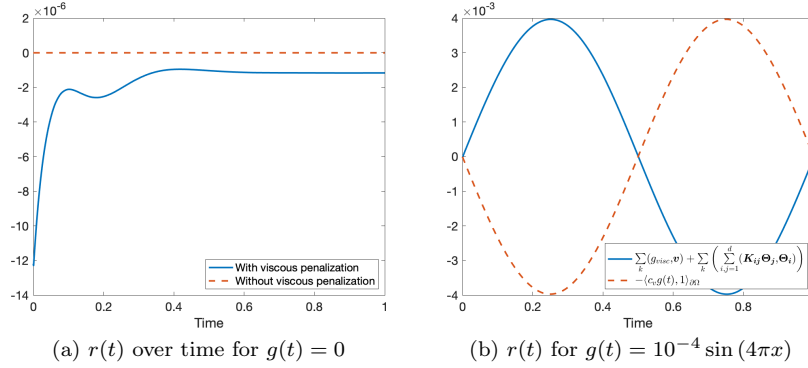


Figure 3: Evolution of $r(t)$ for the lid-driven cavity under zero (adiabatic) and non-zero heat entropy flow $g(t) \neq 0$.

$Ma = .1$, $Re = 1000$, $N = 3$, and $K_{1D} = 16$ to compute the “viscous entropy residual” $r(t)$

$$r(t) = \sum_k \left[(\mathbf{g}_{\text{visc}}, \mathbf{v})_{D^k} + \sum_{i,j=1}^d (\mathbf{K}_{ij} \Theta_j, \Theta_i) \right]. \quad (34)$$

According to Theorem 4.1, $r(t) = \langle c_v g(t), 1 \rangle_{\partial\Omega}$ in the absence of viscous penalization terms. Theorem 4.4 implies that with viscous penalization terms, $r(t)$ should be equal to $\langle c_v g(t), 1 \rangle_{\partial\Omega}$ plus some negative semi-definite quantity which dissipates entropy.

Figure 3a shows the evolution of $r(t)$ over time for $g(t) = 0$ with and without viscous boundary penalization. Without viscous penalization, $r(t)$ is near machine precision. With viscous penalization, $r(t)$ is negative, indicating entropy dissipation. Following [25], we also consider a non-zero heat entropy flow $g(t) = 10^{-4} \sin(4\pi x)$ at the cavity lid. Here, we remove viscous penalization terms and plot both $r(t)$ and the boundary contribution $-\langle c_v g(t), 1 \rangle_{\partial\Omega}$. We observe that the two components are equal and opposite in sign, and adding them together yields a contribution which is again near machine precision.

We now examine the imposition of fixed isothermal conditions. As noted earlier, due to the presence of an additional boundary term, this boundary condition is not provably entropy conservative.

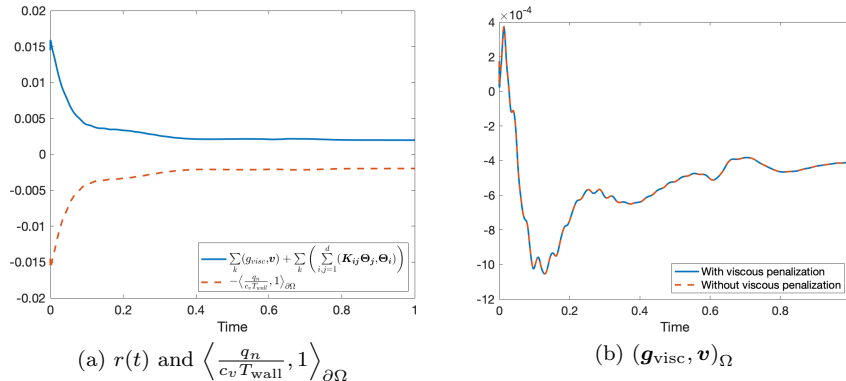


Figure 4: Evolution of the viscous entropy dissipation $(\mathbf{g}_{\text{visc}}, \mathbf{v})_{\Omega}$ and viscous entropy residual $r(t)$ for the lid-driven cavity under an isothermal wall boundary condition of $T = 1$.

However, the formulation used in Theorem 4.2 mimics the continuous entropy inequality, and the resulting simulations appear to remain stable in practice. We note that this mimetic property is not unique to our imposition of boundary conditions, and that the method of imposing isothermal boundary conditions in [25] also semi-discretely mimics the continuous entropy inequality. We verify Theorem 4.2 using an isothermal lid-driven cavity problem with temperature $T = 1$ imposed on all boundaries. The solutions at $T_{\text{final}} = 100$ are nearly identical visually to the solutions in Figure 2, and are not shown for brevity. Figure 4a shows the evolution of the viscous entropy residual $r(t)$ and the boundary contribution $\langle \frac{q_n}{c_v T_{\text{wall}}}, 1 \rangle_{\partial\Omega}$ over time. These two quantities are identical up to machine precision. Finally, Figure 4b shows the viscous entropy dissipation $(\mathbf{g}_{\text{visc}}, \mathbf{v})_{\Omega}$. Since isothermal boundary conditions do not result in provably entropy dissipative boundary contributions, we see that this contribution is positive near the beginning of the simulation.

5.3. Slip wall boundary conditions

We next test the imposition of slip wall boundary conditions. We consider a channel domain $[-2, 2] \times [-1, 1]$ with an adiabatic no-slip wall on the bottom boundary and symmetry boundary conditions on the remaining faces of the channel. We take $\text{Ma} = 1.5$ and $\text{Re} = 100, 1000$ with an initial condition

$$\rho = \begin{cases} 5, & x < 0 \\ 1, & x \geq 0 \end{cases}, \quad u_1 = u_2 = 0, \quad p = \frac{1}{\text{Ma}^2 \gamma} \rho.$$

Figure 5 shows the squared norm of the velocity as well as the evolution of the viscous entropy residual $r(t)$ defined in (34) for a degree $N = 3$ simulation. The domain is meshed using a bisected uniform quadrilateral mesh of $2K_{1D} \times K_{1D}$ elements with $K_{1D} = 16$. No-slip wall effects are clearly visible on the bottom boundary, while the symmetry boundary condition at the top of the domain leaves the shock undisturbed in the normal direction. The viscous entropy residual is zero up to machine precision in the absence of boundary penalization, as predicted by Theorem 4.3. We also observe that adding boundary penalization produces a small amount of entropy dissipation, which is more pronounced near the start of the simulation and for the under-resolved case of $\text{Re} = 1000$.

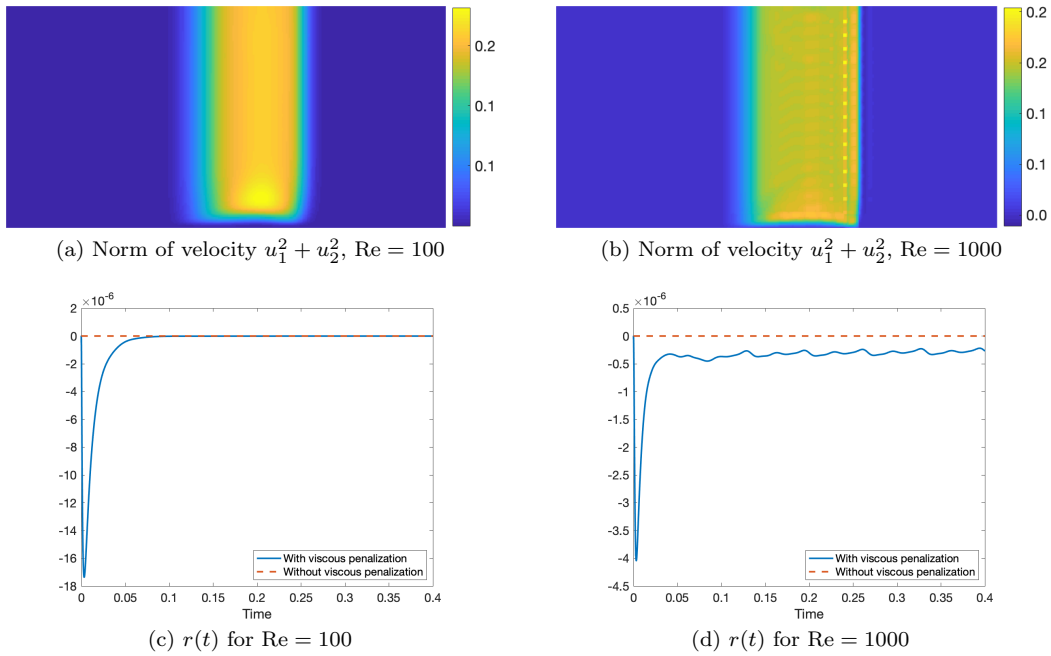


Figure 5: Solutions at time $t = .4$ and evolution of the viscous entropy residual $r(t)$ over time for $Re = 100, 1000$.

5.4. Supersonic flow over a square cylinder

We conclude by investigating supersonic flow from a square cylinder, which includes a variety of physical phenomena including shocks and vorticular features [23, 25]. Following [23, 25], we take $Re = 10^4$ and $Ma = 1.5$ and impose zero adiabatic no-slip solid wall boundary conditions on the cylinder wall. The free-stream values are taken to be

$$\rho = 1, \quad u_1 = 1, \quad u_2 = 0, \quad p = \frac{1}{Ma^2 \gamma}.$$

Both the initial condition and the exterior states on the left, top, and bottom boundaries are set using free-stream values. For the outflow boundary on the right, we utilize a simple “extrapolation” condition and set the exterior value equal to the interior value (we note that this is not provably entropy stable). Figure 6 shows the density for a degree $N = 3$ simulation at $T_{\text{final}} = 100$, as well as the triangular mesh of 16574 elements generated by Gmsh [48]. Shocks and trailing vortices behind the square cylinder are both visible in the numerical solution.

For clearer visualization, we use a color range of $[-.5, 1.5]$. The simulation remains stable without additional artificial viscosity or limiting, though some numerical artifacts are observable (e.g., Gibbs oscillations in the vicinity of shock discontinuities, striations originating from the bow shock).

6. Conclusion

In this paper, we present an entropy stable approach for discretizing viscous terms and enforcing wall boundary conditions for the compressible Navier-Stokes equations. This approach decouples the

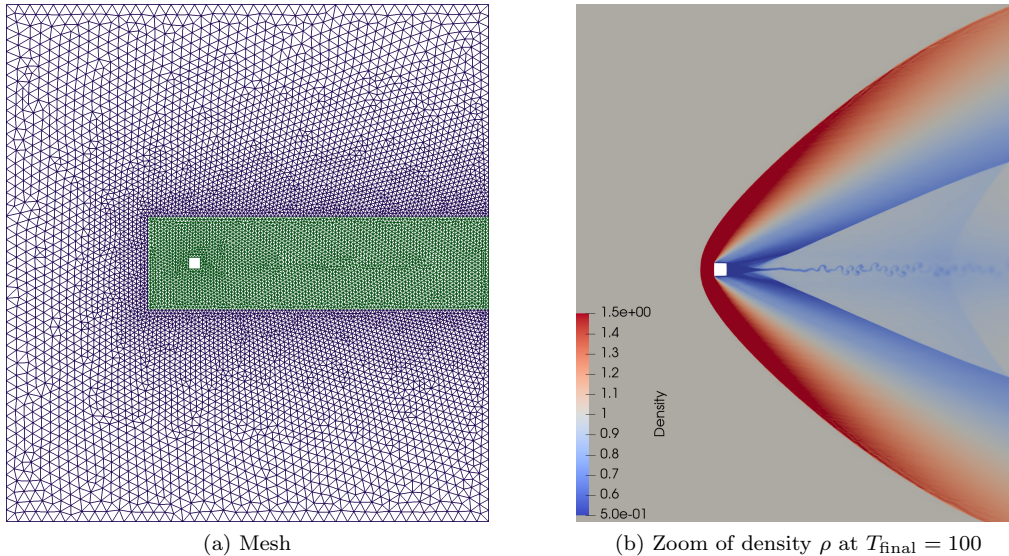


Figure 6: Computational mesh and density ρ at $T_{\text{final}} = 100$ using a degree $N = 3$ approximation.

treatment of volume integrals involving symmetrized viscous coefficient matrices from the treatment of boundary terms, and results in simple and explicit formulas for the entropy stable imposition of no-slip and reflective (slip) boundary conditions.

Acknowledgments

Jesse Chan and Yimin Lin gratefully acknowledge support from the National Science Foundation under award DMS-CAREER-1943186. Tim Warburton was supported in part by the Exascale Computing Project, a collaborative effort of two U.S. Department of Energy organizations (Office of Science and the National Nuclear Security Administration) responsible for the planning and preparation of a capable exascale ecosystem, including software, applications, hardware, advanced system engineering, and early testbed platforms, in support of the nation’s exascale computing imperative. Tim Warburton was also supported in part by the John K. Costain Faculty Chair in Science at Virginia Tech. Finally, the authors thank Matteo Parsani and Lisandro Dalcin for informative discussions.

References

- [1] Jeffrey Slotnick, Abdollah Khodadoust, Juan Alonso, David Darmofal, William Gropp, Elizabeth Lurie, and Dimitri Mavriplis. CFD vision 2030 study: a path to revolutionary computational aerosciences. Technical Report NASA/CR 2014-218178, NASA Langley Research Center, 2014.
- [2] Zhijian J Wang, Krzysztof Fidkowski, Rémi Abgrall, Francesco Bassi, Doru Caraeni, Andrew Cary, Herman Deconinck, Ralf Hartmann, Koen Hillewaert, Hung T Huynh, et al. High-order

- CFD methods: current status and perspective. *International Journal for Numerical Methods in Fluids*, 72(8):811–845, 2013.
- [3] HT Huynh, Zhi J Wang, and Peter E Vincent. High-order methods for computational fluid dynamics: A brief review of compact differential formulations on unstructured grids. *Computers & fluids*, 98:209–220, 2014.
- [4] Mark H Carpenter, Travis C Fisher, Eric J Nielsen, and Steven H Frankel. Entropy Stable Spectral Collocation Schemes for the Navier–Stokes Equations: Discontinuous Interfaces. *SIAM Journal on Scientific Computing*, 36(5):B835–B867, 2014.
- [5] Gregor J Gassner, Andrew R Winters, and David A Kopriva. Split form nodal discontinuous Galerkin schemes with summation-by-parts property for the compressible Euler equations. *Journal of Computational Physics*, 327:39–66, 2016.
- [6] Tianheng Chen and Chi-Wang Shu. Entropy stable high order discontinuous Galerkin methods with suitable quadrature rules for hyperbolic conservation laws. *Journal of Computational Physics*, 345:427–461, 2017.
- [7] Jared Crean, Jason E Hicken, David C Del Rey Fernández, David W Zingg, and Mark H Carpenter. Entropy-stable summation-by-parts discretization of the Euler equations on general curved elements. *Journal of Computational Physics*, 356:410–438, 2018.
- [8] Jesse Chan. On discretely entropy conservative and entropy stable discontinuous Galerkin methods. *Journal of Computational Physics*, 362:346 – 374, 2018.
- [9] Gianmarco Mengaldo, Daniele De Grazia, David Moxey, Peter E Vincent, and Spencer J Sherwin. Dealiasing techniques for high-order spectral element methods on regular and irregular grids. *Journal of Computational Physics*, 299:56–81, 2015.
- [10] Jason E Hicken, David C Del Rey Fernández, and David W Zingg. Multidimensional summation-by-parts operators: general theory and application to simplex elements. *SIAM Journal on Scientific Computing*, 38(4):A1935–A1958, 2016.
- [11] Jesse Chan and Lucas C Wilcox. Discretely entropy stable weight-adjusted discontinuous Galerkin methods on curvilinear meshes. *Journal of Computational Physics*, 378:366 – 393, 2019.
- [12] Jesse Chan. Skew-Symmetric Entropy Stable Modal Discontinuous Galerkin Formulations. *Journal of Scientific Computing*, 81(1):459–485, Oct 2019.
- [13] Matteo Parsani, Mark H Carpenter, Travis C Fisher, and Eric J Nielsen. Entropy Stable Staggered Grid Discontinuous Spectral Collocation Methods of any Order for the Compressible Navier–Stokes Equations. *SIAM Journal on Scientific Computing*, 38(5):A3129–A3162, 2016.
- [14] David C Del Rey Fernández, Jared Crean, Mark H Carpenter, and Jason E Hicken. Staggered-grid entropy-stable multidimensional summation-by-parts discretizations on curvilinear coordinates. *Journal of Computational Physics*, 392:161–186, 2019.
- [15] Jesse Chan, David C Del Rey Fernández, and Mark H Carpenter. Efficient entropy stable Gauss collocation methods. *SIAM Journal on Scientific Computing*, 41(5):A2938–A2966, 2019.

- [16] Jesse Chan, Mario Bencomo, and David C Fernández. Mortar-based entropy-stable discontinuous Galerkin methods on non-conforming quadrilateral and hexahedral meshes. *arXiv preprint arXiv:2005.03237*, 2020.
- [17] Jesse Chan. Entropy stable reduced order modeling of nonlinear conservation laws. *Journal of Computational Physics*, 423:109789, 2020.
- [18] Hendrik Ranocha, Mohammed Sayyari, Lisandro Dalcin, Matteo Parsani, and David I Ketcheson. Relaxation Runge–Kutta methods: fully discrete explicit entropy-stable schemes for the compressible Euler and Navier–Stokes equations. *SIAM Journal on Scientific Computing*, 42(2):A612–A638, 2020.
- [19] Hendrik Ranocha, Lisandro Dalcin, and Matteo Parsani. Fully discrete explicit locally entropy-stable schemes for the compressible Euler and Navier–Stokes equations. *Computers & Mathematics with Applications*, 80(5):1343 – 1359, 2020.
- [20] Gianmarco Mengaldo, Daniele De Grazia, Freddie Witherden, Antony Farrington, Peter Vincent, Spencer Sherwin, and Joaquim Peiro. A guide to the implementation of boundary conditions in compact high-order methods for compressible aerodynamics. In *7th AIAA Theoretical Fluid Mechanics Conference*, page 2923, 2014.
- [21] Magnus Svärd and Jan Nordström. A stable high-order finite difference scheme for the compressible Navier–Stokes equations: no-slip wall boundary conditions. *Journal of Computational Physics*, 227(10):4805–4824, 2008.
- [22] Magnus Svärd and Hatice Özcan. Entropy-stable schemes for the Euler equations with far-field and wall boundary conditions. *Journal of Scientific Computing*, 58(1):61–89, 2014.
- [23] Matteo Parsani, Mark H Carpenter, and Eric J Nielsen. Entropy stable wall boundary conditions for the three-dimensional compressible Navier–Stokes equations. *Journal of Computational Physics*, 292:88–113, 2015.
- [24] Magnus Svärd, Mark H Carpenter, and Matteo Parsani. Entropy stability and the no-slip wall boundary condition. *SIAM Journal on Numerical Analysis*, 56(1):256–273, 2018.
- [25] Lisandro Dalcin, Diego Rojas, Stefano Zampini, David C Del Rey Fernández, Mark H Carpenter, and Matteo Parsani. Conservative and entropy stable solid wall boundary conditions for the compressible Navier–Stokes equations: Adiabatic wall and heat entropy transfer. *Journal of Computational Physics*, 397:108775, 2019.
- [26] Jesse Chan, Leszek Demkowicz, and Robert Moser. A DPG method for steady viscous compressible flow. *Computers & Fluids*, 98:69–90, 2014.
- [27] Thomas JR Hughes, LP Franca, and M Mallet. A new finite element formulation for computational fluid dynamics: I. Symmetric forms of the compressible Euler and Navier-Stokes equations and the second law of thermodynamics. *Computer Methods in Applied Mechanics and Engineering*, 54(2):223–234, 1986.
- [28] David C Del Rey Fernández, Mark H Carpenter, Lisandro Dalcin, Stefano Zampini, and Matteo Parsani. Entropy stable h/p-nonconforming discretization with the summation-by-parts property for the compressible Euler and Navier–Stokes equations. *SN Partial Differential Equations and Applications*, 1(2):1–54, 2020.

- [29] Eitan Tadmor. The numerical viscosity of entropy stable schemes for systems of conservation laws. I. *Mathematics of Computation*, 49(179):91–103, 1987.
- [30] Andrew R Winters, Dominik Derigs, Gregor J Gassner, and Stefanie Walch. A uniquely defined entropy stable matrix dissipation operator for high Mach number ideal MHD and compressible Euler simulations. *Journal of Computational Physics*, 332:274–289, 2017.
- [31] Praveen Chandrashekar. Kinetic energy preserving and entropy stable finite volume schemes for compressible Euler and Navier-Stokes equations. *Communications in Computational Physics*, 14(5):1252–1286, 2013.
- [32] Andrew R Winters, Christof Czernik, Moritz B Schily, and Gregor J Gassner. Entropy stable numerical approximations for the isothermal and polytropic Euler equations. *BIT Numerical Mathematics*, pages 1–34, 2019.
- [33] Xinhui Wu, Jesse Chan, and Ethan J Kubatko. High-order entropy stable discontinuous Galerkin methods for the shallow water equations: curved triangular meshes and GPU acceleration. *arXiv preprint arXiv:2005.02516*, 2020.
- [34] Bernardo Cockburn and Chi-Wang Shu. The local discontinuous Galerkin method for time-dependent convection-diffusion systems. *SIAM Journal on Numerical Analysis*, 35(6):2440–2463, 1998.
- [35] Mohammad Zakerzadeh and Georg May. Entropy stable discontinuous Galerkin scheme for the compressible Navier-Stokes equations. In *55th AIAA Aerospace Sciences Meeting*, page 0084, 2017.
- [36] Bernardo Cockburn and Clint Dawson. Some extensions of the local discontinuous Galerkin method for convection-diffusion equations in multidimensions. In *Proceedings of the Mathematics of Finite Elements and Applications, X, MAFELAP 1999 (Uxbridge)*, pages 225–238. Elsevier, 2000.
- [37] Rommel Bustinza and Gabriel N Gatica. A local discontinuous Galerkin method for nonlinear diffusion problems with mixed boundary conditions. *SIAM Journal on Scientific Computing*, 26(1):152–177, 2004.
- [38] David C Del Rey Fernández, Pieter D Boom, Mark H Carpenter, and David W Zingg. Extension of tensor-product generalized and dense-norm summation-by-parts operators to curvilinear coordinates. *Journal of Scientific Computing*, 80(3):1957–1996, 2019.
- [39] T Warburton. A low-storage curvilinear discontinuous Galerkin method for wave problems. *SIAM Journal on Scientific Computing*, 35(4):A1987–A2012, 2013.
- [40] Douglas N Arnold, Franco Brezzi, Bernardo Cockburn, and L Donatella Marini. Unified analysis of discontinuous Galerkin methods for elliptic problems. *SIAM Journal on Numerical Analysis*, 39(5):1749–1779, 2002.
- [41] Jan S Hesthaven and Tim Warburton. *Nodal discontinuous Galerkin methods: algorithms, analysis, and applications*, volume 54. Springer, 2007.

- [42] Susanne Brenner and Ridgway Scott. *The mathematical theory of finite element methods*, volume 15. Springer Science & Business Media, 2007.
- [43] Florian J. Hindenlang, Gregor J. Gassner, and David A. Kopriva. Stability of Wall Boundary Condition Procedures for Discontinuous Galerkin Spectral Element Approximations of the Compressible Euler Equations. In *Spectral and High Order Methods for Partial Differential Equations ICOSAHOM 2018*, pages 3–19, Cham, 2020. Springer International Publishing.
- [44] John R Dormand and Peter J Prince. A family of embedded Runge-Kutta formulae. *Journal of Computational and Applied Mathematics*, 6(1):19–26, 1980.
- [45] SF Davis. Simplified second-order Godunov-type methods. *SIAM Journal on Scientific and Statistical Computing*, 9(3):445–473, 1988.
- [46] U Ghia, Kirti N Ghia, and CT Shin. High-Re solutions for incompressible flow using the Navier-Stokes equations and a multigrid method. *Journal of Computational Physics*, 48(3):387–411, 1982.
- [47] K-H Chen and RH Pletcher. Primitive variable, strongly implicit calculation procedure for viscous flows at all speeds. *AIAA journal*, 29(8):1241–1249, 1991.
- [48] Christophe Geuzaine and Jean-François Remacle. Gmsh: A 3-D finite element mesh generator with built-in pre-and post-processing facilities. *International Journal for Numerical Methods in Engineering*, 79(11):1309–1331, 2009.